JOURNAL OF THE ATMOSPHERIC SCIENCES

Influence of a fixed tropopause temperature rather than height on axisymmetric Hadley cell theory

SPENCER A. HILL*

Division of Geological and Planetary Sciences, California Institute of Technology, Pasadena, California, and Department of Earth, Planetary, and Space Sciences, University of California, Los Angeles

SIMONA BORDONI

Division of Geological and Planetary Sciences, California Institute of Technology, Pasadena, California

JONATHAN L. MITCHELL

Department of Earth, Planetary, and Space Sciences, and Department of Atmospheric and Oceanic Sciences, University of California, Los Angeles

ABSTRACT

Axisymmetric theory has traditionally assumed that the tropopause height (H_t) is uniform and unchanged from its radiative-convective equilibrium (RCE) value by the emergence of Hadley cells. Recent studies suggest that the tropopause temperature (T_t), not height, is nearly invariant in RCE, which would require appreciable meridional variations in H_t. Here, we derive anew the expressions of axisymmetric theory by assuming a fixed T_t and compare the results to their fixed-H_t counterparts. If T_t and the depth-averaged lapse rate are uniform, H_t must vary linearly with surface temperature, altering the diagnosed gradient-balanced zonal wind at the tropopause appreciably (up to tens of m s^{-1}) but the minimal Hadley cell extent predicted by Hide's theorem only weakly ($\lesssim 1^\circ$). A uniform T_t alters the thermal field required to generate an angular momentum conserving Hadley circulation, but these changes and the resulting changes to the equal-area model solutions for the cell edges again remain quantitative. In numerical simulations of latitude-by-latitude RCE under annual-mean forcing using a single column model, assuming a uniform T_t is reasonably accurate up to the mid-latitudes, and, regardless, the Hide's theorem metrics are again insensitive to how the tropopause is defined. We conclude that, however imperfectly axisymmetric theory models Earth's eddying atmosphere, its treatment of the tropopause is not an important error source.

1. Introduction

Absent a large-scale circulation, local radiative-convective equilibrium (RCE) would necessarily prevail at each latitude: the large-scale meridional and vertical velocities are zero ($v = w = 0$), the lapse rate is adiabatic from the surface to the tropopause, and the interplay between local radiative forcing and convection generates equilibrium temperature and zonal wind fields fields in gradient balance. Provided zonal flow is weak at the surface, the tropopause height then controls the maximum magnitude of the zonal wind within the troposphere at each latitude, $u_\mathrm{t,rce}$. Via Hide's theorem, the resulting absolute angular momentum and absolute vorticity fields determine the emergence (Hide 1969; Schneider 1977; Plumb and Hou 1992) and minimal extent (Held and Hou 1980; Hill et al. 2019) of the Hadley cells in axisymmetric and zonally varying (Emanuel 1995) atmospheres.

The original expressions of Hide's theorem and of the angular momentum conserving (AMC) model of the Hadley cells (Schneider 1977; Held and Hou 1980) were derived in a dry, Boussinesq framework in which the tropopause height, H_t, is assumed uniform in latitude and, if a Hadley circulation emerges, to be unaltered from its RCE value, $H_\mathrm{t,rce}$. This includes the equal-area model for the cell edge locations that combines the AMC assumption with assumptions of temperature continuity and energy conservation within each cell (Held and Hou 1980; Lindzen and Hou 1988). In the adaptation of axisymmetric theory to moist atmospheres obeying convective quasi-equilibrium (CQE; Emanuel et al. 1994; Emanuel 1995), the tropopause height — which appears in temperature coordinates as the difference between the surface and tropopause temperatures, $T_\mathrm{s} - T_\mathrm{t}$ — is not assumed uniform in the expression of Hide's theorem (Eq. 10 of

*Corresponding author address: Spencer Hill, UCLA Department of Earth, Planetary, and Space Sciences, 595 Charles E. Young Dr. East, Los Angeles, CA 90049

E-mail: shill@gps.caltech.edu

Emanuel 1995) but is in deriving the AMC, or "critical", subcloud equivalent potential temperature field (Eq. 11 of Emanuel 1995).

On the one hand, the original, fixed-H_t theories have been remarkably successful for Hadley cells on Earth and other planetary bodies at the conceptual to qualitative levels. On the other, it remains possible that (and, to our knowledge, unexamined whether) appreciable quantitative or even qualitative changes to the results emerge when meridional variations in H_t are accounted for.

That a fixed tropopause height may be problematic can be seen from the hypsometric equation applied over the whole troposphere, $H_t = (R/g)\hat{T}\ln(p_s/p_t)$, where R is the atmospheric gas constant, g is gravity, and $\hat{T}$ is the average temperature from the surface with pressure p_s to the tropopause with pressure p_t. Neglecting surface pressure variations, a given value of H_t will occur at higher pressures (i.e. larger p_t values) in warmer columns compared to cooler columns — opposite to both simulations of RCE (including those presented below) and to observations[1], wherein the tropopause pressure is lowest (and height is highest) in the warmest columns (e.g. Held 1982).

Recent work suggests that the RCE tropopause *temperature*, rather than height, is nearly invariant (Seeley et al. 2019a,b), refining previous arguments that cloud anvils are formed at a fixed temperature both in the tropics (Hartmann and Larson 2002) and extratropics (Thompson et al. 2017, 2018). Absent compensating lapse rate variations, this would cause H_t to vary with surface temperature: given a troposphere-averaged lapse rate $\hat{\Gamma}$, the tropopause height must satisfy

$$H_t = \frac{T_s - T_t}{\hat{\Gamma}}. \tag{1}$$

For a uniform T_t and $\hat{\Gamma}$, H_t varies linearly with T_s — rising on Earth by approximately 1 km per 10 K in dry columns or per ∼6.5 K in moist columns. This immediately resolves the aforementioned problem arising from a fixed tropopause height: $T_s - T_t$, and therefore H_t, must increase with T_s.

Fang and Tung (1994) compare analytical Hadley cell solutions attained with a fixed H_t with or without the tropopause temperature assumed fixed in their linear, viscous model, but this viscous regime is inappropriate for Earth's nearly inviscid troposphere. A fixed T_t is effectively assumed by some idealized general circulation models (GCMs) (e.g. Schneider 2004) used to study the Hadley cells (e.g. Walker and Schneider 2005, 2006; Schneider and Bordoni 2008; Hill et al. 2019), but the implications for the Hadley cells have yet to be explored.

Although Seeley et al. (2019b) demonstrate a rough invariance of the domain-mean tropopause temperature in doubly periodic, fixed-SST, cloud resolving model simulations (i.e. T_t varies by $\lesssim$5 K for SSTs varied from 260 to 310 K), Singh (2019) demonstrates that the RCE meridional distribution of $T_s - T_t$, not T_t, is remarkably uniform in a GCM simulation of latitude-by-latitude RCE [his Figure 5(b)] and across dynamically equilibrated simulations at the cross-equatorial Hadley cell edge at a wide range of rotation rates (his Figure 9). So it remains necessary to assess the validity of a fixed T_t in simulations of latitude-by-latitude RCE.

As is standard, Singh's RCE solutions are computed by re-running the same GCM used to generate the dynamically equilibrated solution but with the large-scale advective tendencies set to zero. The results are certainly prognostic in that they do not require knowledge of the dynamically equilibrated simulations, but in practice they still require running a GCM (with the added burden of modifying the source code to inhibit large-scale transports). An analytical solution that captures the RCE fields of relevance to the Hadley cells would be preferable.

These considerations motivate the present study. We begin by demonstrating that, based on (1), meridional tropopause height variations can indeed be large under both annual-mean and more solstice-like forcings (Section 2). We then derive a new expression for $u_{t,rce}$ that assumes a fixed T_t, compare it to its fixed-H_t counterpart (Section 3), and investigate the resulting influences on the three conditions (Adam and Paldor 2010; Hill et al. 2019) of Hide's theorem for the emergence and minimal extent of the Hadley circulation (Section 4). In a similar progression, we then derive fixed-T_t forms of the AMC thermal fields (Section 5) and explore the resulting impacts on the equal-area model (Section 6). We then construct annual-mean latitude-by-latitude RCE conditions via single-column model simulations to assess whether a meridionally uniform T_t is plausible, the sensitivity of $u_{t,rce}$ and the Hadley cell metrics to the tropopause definition, and how accurately the numerical results can be captured by a very simple analytical approximation (Section 7).

As fully summarized in Section 8, we find that the results of axisymmetric theory are remarkably insensitive to how the tropopause is treated. This should add to the community's confidence in the original axisymmetric theories, an implication we discuss with others in Section 9.

2. Effect of a fixed T_t on the tropopause height in latitude-by-latitude RCE

Figure 1 shows H_t diagnosed using (1) assuming T_t = 200 K, a uniform lapse rate of $\Gamma = \gamma\Gamma_d$, where $\Gamma_d = g/c_p$ is the dry adiabatic lapse rate and $\gamma = 0.65$, and a troposphere-averaged potential temperature distribution, $\hat{\theta}_{rce}$, given by the canonical troposphere-averaged forcing

[1]The observed tropopause structure reflects both dynamical and radiative influences, which makes comparing it with these purely RCE-based arguments imperfect.

of Lindzen and Hou (1988):

$$\frac{\hat{\theta}_{\rm rce}}{\theta_0} = 1 + \frac{\Delta_{\rm h}}{3}\left[1 - 3(\sin\varphi - \sin\varphi_{\rm m})^2\right]. \qquad (2)$$

In (2), the forcing maximizes at the latitude $\varphi_{\rm m}$ set to either 0, 6, or 23.5°N, $\Delta_{\rm h}$ is an imposed fractional planetary-scale temperature contrast set to 1/6, and the Boussinesq reference potential temperature θ_0 is set to 290 K. The surface temperature is then solved for from Γ and $\hat{\theta}_{\rm rce}$ in a manner described in the following section.

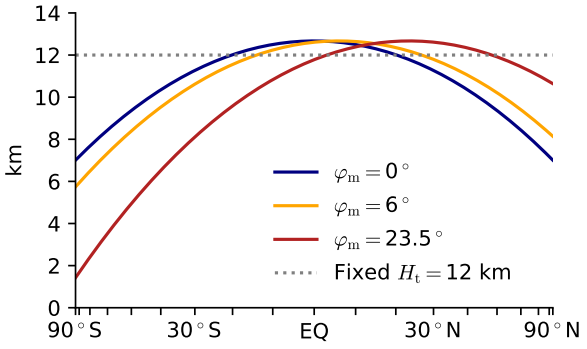

FIG. 1. Tropopause height in the RCE state given by (2) with the forcing maximum latitude $\varphi_{\rm m}$ value according to the legend, assuming a uniform tropopause temperature of 200 K and a uniform lapse rate of $\gamma\Gamma_{\rm d}$, with $\gamma = 0.65$. For comparison, the dotted grey line shows a hypothetical tropopause with uniform height of 12 km.

In the annual-mean case of $\varphi_{\rm m} = 0°$, the RCE tropopause height is ∼13 km at the equator and decreases to ∼10 km at ±30° and ∼7 km at the poles. As the forcing maximum latitude is moved into the Northern Hemisphere, by construction the tropopause height at $\varphi_{\rm m}$ remains ∼13 km, but the tropopause drops to successively lower values in the southern, winter hemisphere. The $\varphi_{\rm m} = 23.5°$ case reveals the likely over-simplicity of this expression, with $H_{\rm t}$ dropping below 2 km at the poles; for $\varphi_{\rm m}$ sufficiently farther poleward (not shown), $T_{\rm s}$ drops below $T_{\rm t}$ near the winter pole, yielding the fallacious prediction of a vanishing or negative tropopause height.

Nevertheless, restricting to low- to mid-latitudes where the results are more reasonable and of more relevance to the Hadley cells, $H_{\rm t}$ varies meridionally by up to ∼5 km, i.e. by ∼40% — variations sufficiently large to motivate examining their influence on $u_{\rm t,rce}$.

3. Effect of a fixed $T_{\rm t}$ on the gradient-balanced zonal wind at the tropopause

a. Roadmap

For the fixed-$T_{\rm t}$ derivations and all figures in this and subsequent sections through Section 6, we use the Boussinesq framework. As above, we assume a $\hat{\theta}_{\rm rce}$ field given by (2), although we deviate from the vertical thermal structure assumed by Held and Hou (1980) and Lindzen and Hou (1988) by assuming that, as above, $\Gamma = \gamma\Gamma_{\rm d}$, setting $\gamma = 0.65$ to mimic the stabilizing effects of moist convection.[2] As will be shown in tables below, results regarding the Hadley cells' sensitivity to whether $H_{\rm t}$ or $T_{\rm t}$ is assumed fixed are essentially unchanged if the atmosphere is dry (i.e. $\gamma = 1$) or if the CQE system of equations is used instead. That results are similar between the Boussinesq and CQE cases can be partly understood based on Appendix A, which provides a derivation of $u_{\rm t,rce}$ in the CQE system, compares it to the corresponding Boussinesq expression, and shows that the original, Boussinesq form of the angular momentum conserving model of the Hadley cell amounts to a linearization of the corresponding CQE solution about the cell's ascent latitude.

Finally, all of the concepts from axisymmetric theory considered from here through Section 6 are described in detail by Hill et al. (2019). We provide short summaries at the start of each section here and refer readers to that study for details.

b. Sensitivity of $u_{\rm t,rce}$ to a fixed tropopause height vs. temperature

The gradient-balanced zonal wind at the tropopause in a state of latitude-by-latitude RCE may be written

$$u_{\rm t,rce} = \Omega a\cos\varphi\left[\sqrt{1 - \frac{1}{\cos\varphi\sin\varphi}\frac{gH_{\rm t}}{\Omega^2 a^2\theta_0}\frac{\partial\hat{\theta}_{\rm rce}}{\partial\varphi}} - 1\right] \qquad (3a)$$

where Ω is the planetary rotation rate, and a is planetary radius. Using (1) and assuming a fixed $T_{\rm t}$ and $\Gamma = \gamma\Gamma_{\rm d}$, (3a) becomes

$$u_{\rm t,rce} = \Omega a\cos\varphi\left[\sqrt{1 - \frac{1}{\cos\varphi\sin\varphi}\frac{c_p(T_{\rm s} - T_{\rm t})}{\gamma\Omega^2 a^2\theta_0}\frac{\partial\hat{\theta}_{\rm rce}}{\partial\varphi}} - 1\right]. \qquad (3b)$$

Understanding how $u_{\rm t,rce}$ may differ between these two expressions is easiest for dry atmospheres, in which $\gamma = 1$ and thus $T_{\rm s} = \theta = \hat{\theta}$: where $T_{\rm s}$ is relatively warm, $T_{\rm s} - T_{\rm t}$ is

[2] By construction, there is no dependence of $\hat{\theta}_{\rm rce}$ on $H_{\rm t,rce}$ with the original vertical structure used by Held and Hou (1980) and Lindzen and Hou (1988), i.e. $\theta_{\rm rce}(z)/\theta_0 = \cdots + \Delta_{\rm v}(z/H_{\rm t} - 1/2)$, where $\Delta_{\rm v}$ is an imposed fractional potential temperature increase from the surface to the tropopause, set to 1/8 in their studies. Assuming $p_{\rm s} = p(z=0) = p_0$, it can be shown that this implies a lapse rate of

$$\frac{{\rm d}T}{{\rm d}z} = \frac{\theta_0\Delta_{\rm v}}{H_{\rm t}} - \Gamma_{\rm d}\left[1 + \frac{R_{\rm d}}{c_p}\ln\left(\frac{p_0}{p}\right)\right].$$

Using the parameter values from Lindzen and Hou (1988), namely $\theta_0 = 300$ K, $\Delta_{\rm v} = 1/8$, and $H_{\rm t} = 15$ km, this yields effective γ values ranging from roughly 0.7 to 0.9, with the lapse rate decreasing moving vertically upward and poleward away from the forcing maximum (not shown). All else equal, vertically averaged lapse rates with $\gamma \approx 0.65$ would require $\Delta_{\rm v} \approx 1/4$ (not shown).

relatively large, and thus $u_{\mathrm{t,rce}}$ is larger in magnitude than it would be for a fixed H_t. In moist atmospheres, the stable stratification causes θ to increase with height, and thus $\hat{\theta}$ exceeds T_s, the more so the deeper the tropopause or the steeper the lapse rate. More formally, it can be shown that, if $\Gamma = \gamma\Gamma_\mathrm{d}$ and ignoring differences between surface pressure and the reference pressure appearing in the potential temperature, then $\theta(z) = {T_\mathrm{s}}^{1/\gamma}(T_\mathrm{s} - \gamma\Gamma_\mathrm{d} z)^{1-1/\gamma}$, and therefore that

$$\hat{\theta} = \frac{\gamma}{2\gamma - 1}\frac{{T_\mathrm{s}}^{1/\gamma}}{T_\mathrm{s} - T_\mathrm{t}}\left({T_\mathrm{s}}^{2-1/\gamma} - {T_\mathrm{t}}^{2-1/\gamma}\right). \tag{4}$$

As such, a fixed tropopause temperature (and lapse rate) alter $u_{\mathrm{t,rce}}$ via an additional pathway in stably stratified Boussinesq atmospheres, namely by altering $\partial_\varphi \hat{\theta}_\mathrm{rce}$.

(3b) is not a closed expression for a given $\hat{\theta}_\mathrm{rce}$ unless T_s is known. The simplest approach is to neglect the difference between T_s and $\hat{\theta}$, assuming $T_\mathrm{s} \approx \hat{\theta}_\mathrm{rce}$. But for moist atmospheres ($\gamma < 1$), this yields an overestimation of $T_\mathrm{s} - T_\mathrm{t}$, and with it $u_{\mathrm{t,rce}}$, that if used artificially inflates the seeming difference between results from the fixed-H_t and fixed-T_t expressions (not shown). Therefore, we use the specified values of $\hat{\theta}_\mathrm{rce}$ [from (2)], γ, and T_t (set to 0.65 and 200 K, respectively) to numerically solve (4) for T_s (including in the calculation of H_t in Figure 1 discussed above).

Figure 2(a) shows $u_{\mathrm{t,rce}}$ diagnosed using (3a) vs. (3b) for φ_m equal to 0, 6, or 23.5°N. For the fixed-H_t calculations, the value of H_t is taken to be the 30°S-30°N average H_t value from the corresponding fixed-T_t calculation. For the annual-mean-like case ($\varphi_\mathrm{m} = 0°$), the tropopause's maximum height at the equator and its monotonic decrease toward either pole makes $u_{\mathrm{t,rce}}$ more westerly than the fixed-H_t case in the region where the fixed-T_t tropopause height exceeds its tropical mean value, from the equator to ∼20°S/N, but only by $\lesssim$3 m s^{-1}. Poleward thereof, the tropopause height is lower than its tropical-mean value, and this reduces $u_{\mathrm{t,rce}}$ compared to the fixed-H_t formulation by up to 5 m s^{-1}.

For the solstice-like cases ($\varphi_\mathrm{m} = 6, 23.5°$), the relatively deep tropopause near φ_m very slightly increases the magnitudes of both the easterlies on its equatorward side within the summer hemisphere and the westerlies on its poleward side. In the winter hemisphere, the westerlies are weakened more appreciably — up to ∼20 m s^{-1} in the mid-latitudes and by ∼10 m s^{-1} in the subtropics for $\varphi_\mathrm{m} = 23.5°$ — due to a comparatively low tropopause height locally.

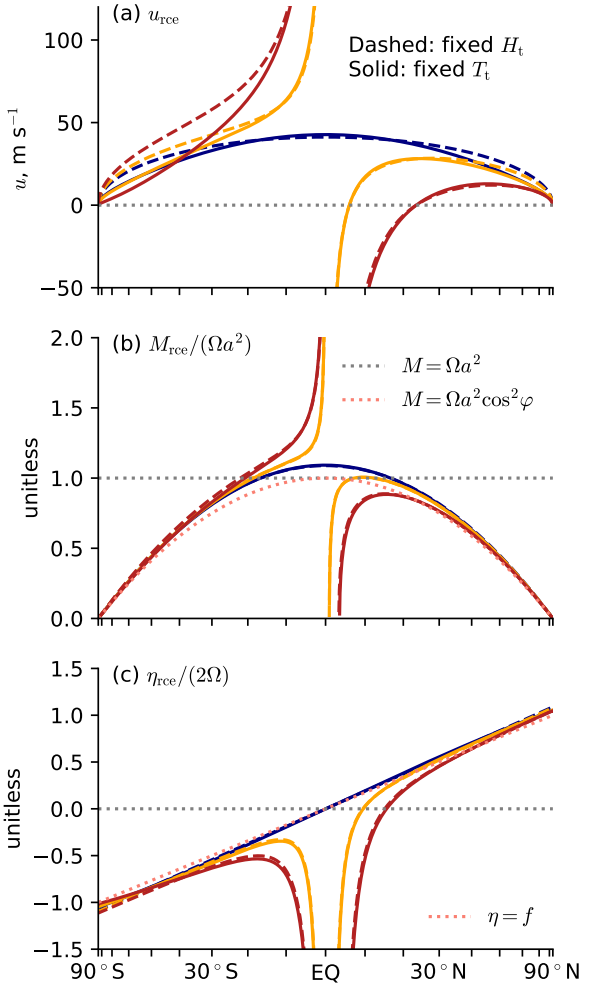

FIG. 2. At the local tropopause, (a) zonal wind in m s^{-1}, (b) absolute angular momentum normalized by the equatorial planetary angular momentum, and (c) absolute vorticity normalized by 2Ω in the RCE state given by (2) with the forcing maximum latitude φ_m value according to the legend in (a), with either the tropopause (dashed) height or (solid) temperature assumed constant. The fixed-height calculations use the 30°S-30°N average tropopause height from the corresponding fixed-temperature calculation (all of which set $T_\mathrm{t} = 200$ K). Overlaid in (b) are (dotted gray) the equatorial planetary angular momentum and (dotted pink) the local planetary angular momentum. Overlaid in (c) are (dotted gray) the $\eta = 0$ curve (which would correspond to uniform angular momentum, e.g. the dotted grey curve in (b)), and (dotted pink) the planetary vorticity, i.e. $\eta = f$.

4. Effect of a fixed T_t on the minimal Hadley cell extent based on Hide's theorem

Given $u_{\mathrm{t,rce}}$, any isolated extremum in the corresponding absolute angular momentum field, $M_{\mathrm{t,rce}} = a\cos\varphi(\Omega a\cos\varphi + u_{\mathrm{t,rce}})$ or (nearly equivalently) any sign change within either hemisphere in the corresponding absolute vorticity field, $\eta_{\mathrm{t,rce}} = -(a^2\cos\varphi)^{-1}\partial_\varphi M_{\mathrm{t,rce}} = f - a^{-1}\partial_\varphi u_{\mathrm{t,rce}}$, is physically impossible (Hide 1969; Schneider 1977; Plumb and Hou 1992; Emanuel 1995). Therefore, a Hadley cell must emerge if the RCE state exhibits any of $M_{\mathrm{t,rce}} > \Omega a^2$, $M < 0$, or $f\eta_{\mathrm{t,rce}} < 0$ at any latitude (Ωa^2 and 0 being the

extremal planetary values of angular momentum, at the equator and either pole, respectively), and at the very least the resulting circulation must span all latitudes meeting any of these three conditions of Hide's theorem. For annual-mean-like forcing, only the $M_{\mathrm{t,rce}} > \Omega a^2$ condition is typically met; for solstice-like forcing, typically the $M_{\mathrm{t,rce}} > \Omega a^2$ condition is met over some appreciable range of the winter hemisphere, the $M_{\mathrm{t,rce}} < 0$ condition is met in a narrow range near the equator in the summer hemisphere, and the $f\eta_{\mathrm{t,rce}} < 0$ condition is met over some appreciable range poleward thereof (except under exotic forcings, c.f. Hill et al. 2019), making where $\eta_{\mathrm{t,rce}} = 0$ in the summer hemisphere a lower bound on how far the Hadley circulation extends into the summer hemisphere.

Directly at the equator, these emergence metrics are unaffected by meridional variations in H_{t}: a $\hat{\theta}_{\mathrm{rce}}$ maximum still yields equatorial westerlies and thus $M_{\mathrm{t,rce}} > \Omega a^2$ locally, and a nonzero cross-equatorial $\hat{\theta}_{\mathrm{rce}}$ gradient still cannot be balanced, yielding $M_{\mathrm{t,rce}} > \Omega a^2$ on the winter side and $M_{\mathrm{t,rce}} < 0$ on the summer side of the equator. But, away from the equator, the $M_{\mathrm{t,rce}} > \Omega a^2$, $M_{\mathrm{t,rce}} < 0$, and $f\eta_{\mathrm{t,rce}} < 0$ extents are all in principle altered by the tropopause treatment.

Figure 2(b) shows $M_{\mathrm{t,rce}}$ computed for the $\varphi_{\mathrm{m}} = 0, 6, 23.5^\circ$, $\gamma = 0.65$ cases discussed already, with either H_{t} or T_{t} fixed, and Table 1 shows the maximal poleward extent of each Hide's theorem metric. For $\varphi_{\mathrm{m}} = 0^\circ$ and $\varphi_{\mathrm{m}} = 6^\circ$, the $M_{\mathrm{t,rce}} > \Omega a^2$ extent is essentially unchanged by the fixed-T_{t} formulation. For $\varphi_{\mathrm{m}} = 23.5^\circ$, the summer hemisphere westerlies are far enough poleward (where the planetary M values are lower) that neither the fixed-H_{t} nor fixed-T_{t} calculations of $M_{\mathrm{t,rce}}$ exceed Ωa^2 in the summer hemisphere, and in the winter hemisphere its extent contracts equatorward by a nontrivial but still quantitative 1.3°.

Figure 2(c) shows the corresponding calculations of $\eta_{\mathrm{t,rce}}$, and Table 1 shows the $\eta_{\mathrm{t,rce}} = 0$ locations for the off-equatorial forcing maximum cases [c.f. Hill et al. (2019), the $M_{\mathrm{t,rce}} < 0$ and $f\eta_{\mathrm{t,rce}} < 0$ conditions are never met in the $\varphi_{\mathrm{m}} = 0$ case]. For $\varphi_{\mathrm{m}} = 6^\circ$, westerlies occurring just poleward of φ_{m} are sufficiently strong as to generate a local $M_{\mathrm{t,rce}}$ maximum poleward of φ_{m} that slightly exceeds the local planetary M value with either tropopause treatment, and this maximum moves only from 9.4° to 9.5° when the fixed-T_{t} assumption is introduced. For $\varphi_{\mathrm{m}} = 23.5^\circ$, the local $M_{\mathrm{t,rce}}$ maximum is generated equatorward of φ_{m} at a value less than the local planetary M value, driven by strong easterlies, and this moves from 15.1° to 15.6° when a fixed-T_{t} is assumed.

Table 1 also shows the Hide's theorem metrics for the corresponding Boussinesq $\gamma = 1$ and CQE cases. In the moist case compared to the dry case, the shallower lapse rate leads to a deeper tropopause, and with it larger $u_{\mathrm{t,rce}}$ values, and thus wider Hadley cell metrics. In fact, these differences between the dry and moist Boussinesq cases for a given tropopause treatment are generally larger than are the differences between the two tropopause treatments for either the dry case or the moist case. Results are also similar for the CQE framework, with only quantitative changes to the Hide's theorem metric extents when computed assuming a fixed T_{t}. With either a fixed H_{t} or T_{t}, the CQE values are closer to their dry Boussinesq counterparts than to their moist Boussinesq counterparts, with the moist Boussinesq metrics generally farther poleward; the same holds for the AMC results discussed in subsequent sections.

What explains this relative insensitivity of the Hide's theorem metrics to the tropopause meridional structure? For the $\varphi_{\mathrm{m}} = 0^\circ$ case, $u_{\mathrm{t,rce}}$ is only altered by up to $\sim 3\ \mathrm{m\ s^{-1}}$, making the insensitivity unsurprising. But even if the differences were larger in magnitude, the $M_{\mathrm{t,rce}} = \Omega a^2$ point happens to occur within a few degrees latitude of where the fixed-T_{t} tropopause height goes from being greater-than to less-than its tropical-mean value used in the fixed-H_{t} calculations (c.f. Figure 1). So $u_{\mathrm{t,rce}}$, and in turn $M_{\mathrm{t,rce}}$, is only modestly affected in the region of relevance. A similar phenomenon occurs for the $\eta_{\mathrm{t,rce}} = 0$ metric in the off-equator forcing cases. By construction, $u_{\mathrm{t,rce}} = 0$ at φ_{m} regardless of the tropopause structure, and in the cases shown the $\eta_{\mathrm{t,rce}} = 0$ is not far removed from φ_{m}. The effects of the tropopause treatment on $u_{\mathrm{t,rce}}$, and in turn $M_{\mathrm{t,rce}}$ and $\eta_{\mathrm{t,rce}}$, in the vicinity are accordingly modest. In contrast, for $\varphi_{\mathrm{m}} = 23.5^\circ$, the winter hemisphere $M_{\mathrm{t,rce}} = \Omega a^2$ point occurs where the fixed-T_{t} tropopause height differs more appreciably from its tropical mean, yielding a nontrivial difference between the fixed height vs. temperature calculations.

This ultimately depends on the H_{t} value chosen for the fixed-H_{t} calculations, which is admittedly somewhat arbitrary. But, to us, the tropical mean value from the fixed-T_{t} solutions seems like the most appropriate — i.e. the least likely to artificially inflate the seeming difference between the two formulations.

5. Effect of a fixed T_{t} on the angular momentum conserving model

Assuming that any of the three Hide's theorem conditions is met at any latitude (as can be expected nearly always, c.f. Schneider 2006; Hill et al. 2019), the latitude-by-latitude RCE state is impossible, and a Hadley circulation must emerge. Provided that drag is strong in the boundary layer but viscosity and eddy stresses are weak in the free troposphere, air parcels ascending out of the boundary layer will conserve the local planetary angular momentum value as they circulate. If this ascent is concentrated into a narrow convergence zone at the latitude φ_{a}, the Hadley cell will then exhibit the AMC zonal wind profile $u_{\mathrm{amc}} = \Omega a \cos\varphi (\cos^2\varphi_{\mathrm{a}}/\cos^2\varphi - 1)$ and a

TABLE 1. Metrics from Hide's theorem indicating minimal Hadley cell extent (in degrees latitude) computed using either the traditional, fixed-height equations or the new, fixed-temperature equations. Also shown for each forcing maximum latitude value is the value (in km) used for the fixed-H_t calculations, namely the tropopause height averaged over 30°S-30°N given that forcing and assuming a fixed T_t.

		Boussinesq, dry		Boussinesq, moist		CQE	
φ_m	Metric	Fixed H_t	Fixed T_t	Fixed H_t	Fixed T_t	Fixed H_t	Fixed T_t
0°	$\overline{H_t}$		10.4 km		12.2 km		x.x km
	$M_{t,rce} > \Omega a^2$	15.5°	15.5°	16.6°	16.6°	x.x°	x.x°
6°	$\overline{H_t}$		10.4 km		12.1 km		x.x km
	$M_{t,rce} > \Omega a^2$, summer	10.0°	10.6°	11.9°	12.3°	x.x°	x.x°
	$M_{t,rce} > \Omega a^2$, winter	-17.6°	-17.4°	-18.8°	-18.5°	x.x°	x.x°
	$M_{t,rce} < 0$	0.8°	0.8°	0.9°	1.0°	x.x°	x.x°
	$f\eta_{t,rce} < 0$	9.0°	9.1°	9.4°	9.5°	x.x°	x.x°
23.5°	$\overline{H_t}$		9.7 km		11.3 km		x.x km
	$M_{t,rce} > \Omega a^2$, winter	-20.9°	-19.7°	-22.0°	-20.7°	x.x°	x.x°
	$M_{t,rce} < 0$	2.9°	3.1°	3.4°	3.5°	x.x°	x.x°
	$f\eta_{t,rce} < 0$	14.3°	14.8°	15.1°	15.6°	x.x°	x.x°

corresponding gradient-balanced AMC thermal field $\hat{\theta}_{amc}$ (Held and Hou 1980; Lindzen and Hou 1988) given by — if H_t is uniform —

$$\frac{\hat{\theta}_{amc}(\varphi) - \hat{\theta}_a}{\theta_0} = -\frac{\Omega^2 a^2}{2gH_t}\frac{(\cos^2\varphi_a - \cos^2\varphi)^2}{\cos^2\varphi}, \qquad (5a)$$

where $\hat{\theta}_a$ is the value of $\hat{\theta}_{amc}$ at φ_a. At minimum, the resulting AMC Hadley circulation must span all latitudes where $u_{amc} < u_{t,rce}$; otherwise a local extremum in $M_{t,rce}$ would still exist at the cell edge in violation of Hide's theorem — a typically broader expanse than the minimal extent directly set by Hide's theorem discussed in previous sections that is agnostic to the dynamically equilibrated zonal wind field.

In the previous sections relating to the hypothetical RCE state, the RCE thermal field was taken as given, and the task at hand was to determine how tropopause height variations alter the zonal wind field. For the AMC model, the converse is required: the AMC wind u_{amc} does not vary with height in thin-shell atmospheres, and it is the column-averaged temperature field in gradient balance with u_{amc}, $\hat{\theta}_{amc}$, that may be altered by a fixed T_t. To be clear, the original fixed-T_t argument (Seeley et al. 2019b) applies strictly to RCE, not to the tropopause in the presence of a large-scale circulation that alters the tropopause structure through its own dynamical influences (Held 1982). Nevertheless, as a limiting case and for the sake of analytical tractability, we assume uniform values of T_t and $\hat{\Gamma}$ within the Hadley cells equal to their RCE values.

For the fixed-T_t, $\Gamma = \gamma\Gamma_d$ case, we show in Appendix B that, to a good approximation, the AMC surface temperature is

$$T_{s,amc} = T_t + \sqrt{(T_{sa} - T_t)^2 - \frac{\gamma\theta_0\Omega^2 a^2}{c_p d\hat{\theta}/dT_s}\frac{(\cos^2\varphi_a - \cos^2\varphi)^2}{\cos^2\varphi}}, \qquad (5b)$$

where T_{sa} is the value of T_s at φ_a. We have assumed that $d\hat{\theta}/dT_s$ is constant, using a value of 1.4 (see Appendix B for justification), and that $p_s \approx p_0 = 1000$ hPa at all latitudes. The $\hat{\theta}_{amc}$ field can then be computed by plugging (5b) into (4). The fixed-T_t $\hat{\theta}_{amc}$ becomes undefined once the surface temperature drops to T_t, since this would imply a vanishing tropopause height.

Figure 3 shows the RCE and AMC tropopause height and column-integrated potential temperature, with either fixed-H_t or fixed-T_t assumed, for each of the $\varphi_m = 0, 6, 23.5°$ RCE cases discussed in previous sections. For each AMC solution, φ_a is determined from the equal-area model discussed in the next section. As was the case for the RCE state, a fixed T_t and lapse rate forces H_t to have the same meridional structure as T_s, including the equatorial minimum for $\varphi_a \neq 0$ cases. In the $\varphi_a = 0$ case, this leads to a very flat tropopause height in low latitudes. In all cases, a sharp shoulder emerges in H_t poleward of φ_a in the summer hemisphere and $-\varphi_a$ in the winter hemisphere, occurring in the subtropics for $\varphi_m = 0$ and farther toward mid-latitudes as φ_m is increased.

These shoulders in H_t, in turn, sharpen the corresponding shoulders of $\hat{\theta}_{amc}$. But ultimately this effect is modest (only a few Kelvin), and within the core of the Hadley cells it is weaker still.

Table 2 lists the locations of the $u_{amc} = u_{t,rce}$ points controlling the minimal AMC Hadley cell extent, for the moist Boussinesq, dry Boussinesq, and CQE frameworks for each φ_m value. The derivation of the CQE fixed-T_t solution differs from the Boussinesq derivation yielding (5b) and is presented in Appendix C. For all three, under annual-mean forcing values are essentially unchanged going from a fixedH_t to a fixed T_t. For $\varphi_m = 6°$, the summer hemisphere minimal extent is moved slightly poleward by a fixed T_t ($\leq 0.3°$), but the winter hemisphere extent is moved equatorward by nearly the same amount. For $\varphi_m = 23.5°$, the summer hemisphere $u_{t,rce} = u_{amc}$ point oc-

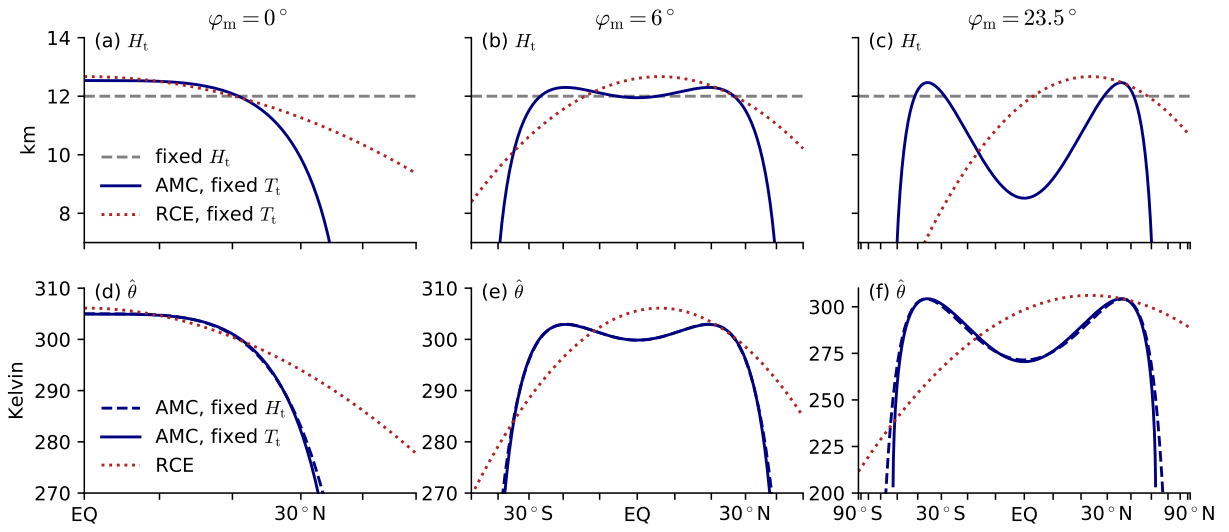

FIG. 3. (top row) Tropopause height and (bottom row) troposphere-averaged potential temperature corresponding to the RCE state given by (2), with the forcing maximum latitude φ_m set to (columns, left to right) 0, 6, or 23.5°, or to the angular momentum conserving (AMC) model, with the ascent latitudes used for the AMC solutions computed using the equal-area model applied to the given RCE potential temperature profile, and with either the tropopause (dashed) height or (solid) temperature assumed fixed. Note differing horizontal axis ranges in each column and differing vertical axis ranges across panels in the bottom row. Results shown are for the Boussinesq model with uniform lapse rate $\Gamma = \gamma\Gamma_d$, with $\gamma = 0.65$; differences between the fixed-height and fixed-temperature calculations are similarly modest in the Boussinesq model with $\gamma = 1$ or in the CQE model (not shown).

curs exactly at φ_m itself, where both fields equal zero: unlike the $\varphi_m = 6^\circ$ case, u_{amc} is increasing moving poleward more rapidly than is $u_{t,rce}$ directly at and everwhere poleward of φ_m. In contrast, the $\varphi_m = 23.5^\circ$ winter hemisphere minimal poleward extent decreases by 1.4-1.5°, due to the weakened $u_{t,rce}$ westerlies (c.f. Table 1).

6. Effect of a fixed T_t on the equal-area model

The equal-area model assumes that the Hadley cells are angular momentum conserving, that column-averaged temperature is continuous at all cell edges (which requires the Hadley cell temperatures to equal the RCE temperatures at the circulation's outer edges), and that the cells conserve energy in the sense that the potential temperature integrated over the extent of each cell is the same as it was over that extent in the RCE state (Held and Hou 1980; Lindzen and Hou 1988). It predicts, given only the knowledge of the RCE potential temperature distribution, the locations of all three Hadley cell edges (the two poleward edges and φ_a) and the temperature at φ_a.

Figure 4 shows the equal-area model solutions for the three cell edges for φ_m varied from 0.1 up to 23.5°, with the AMC temperature fields constructed either using (5a) (with $H = 12$ km) or (5b) (with $T_t = 200$ K), and with all other parameters Earth-like. And Table 2 lists these values and the corresponding $\hat{\theta}_a$ solutions for the $\varphi_m = 0, 6, 23.5^\circ$ cases. Because going from fixed-H_t to fixed-T_t tends to sharpen the subtropical shoulder in $\hat{\theta}_{amc}$, the equal-area solutions for the cell poleward edges typically move equatorward, the more so the farther poleward φ_m is and more so in the winter- than summer hemisphere (c.f. Table 2, for $\varphi_m = 6^\circ$ the summer hemisphere edge actually moves slightly poleward). And φ_a moves either very weakly ($\varphi_m = 6^\circ$) or modestly equatorward ($\varphi_m = 23.5^\circ$).

Table 2 also lists the dry Boussinesq and CQE equal-area values. As with all previously discussed results, the influence of the tropopause treatment is almost always of the same sign and of similar magnitudes across the three formulations. The largest change in total Hadley cell extent occurs for $\varphi_m = 23.5^\circ$ in the CQE system, for which the winter edge retreats equatorward by 3° and the summer edge by 0.9°, for a nontrivial 3.9° total. However, as discussed by Hill et al. (2019) and can be gleaned from Figure 4,[3] the equal-area-predicted cell extents become clearly excessive as φ_m is moved beyond a few degrees of the equator, making this 3.9° difference of less practical importance.

Also overlaid in Figure 4 are the $\eta_{t,rce} = 0$ locations assuming either fixed-H_t or fixed-T_t in Figure 4. As φ_m moves poleward and the overall predicted Hadley circulation grows, $\eta_{t,rce} = 0$ falls equatorward of φ_m and becomes increasingly separated from φ_a (Hill et al. 2019), and this is insensitive to the tropopause treatment.

[3] Note that Hill et al. (2019) set Δ_h to 1/3 as in Held and Hou (1980) rather than 1/6 as in Lindzen and Hou (1988) and the present study; for a given φ_m value, a larger meridional temperature drop yields wider cells and a more poleward φ_a.

TABLE 2. The $u_{\mathrm{amc}} = u_{\mathrm{t,rce}}$ lower bound on Hadley cell extent and the predicted Hadley cell edges from the equal-area model (all in degrees latitude) computed using either the traditional, fixed-height equations or the new, fixed-tropopause temperature equations.

		Boussinesq, dry		Boussinesq, moist		CQE	
φ_{m}	Metric	Fixed H_{t}	Fixed T_{t}	Fixed H_{t}	Fixed T_{t}	Fixed H_{t}	Fixed T_{t}
0°	$u_{\mathrm{t,rce}} = u_{\mathrm{amc}}$	15.5°	15.5°	16.6°	16.6°	15.5°	15.5°
	Equal area φ_{s}	19.5°	18.7°	21.2°	20.5°	19.4°	18.4°
	Equal area $\hat{\theta}_{\mathrm{a}}$ or $\theta_{\mathrm{eb,a}}$	305.2 K	305.2 K	305.0 K	304.9 K	305.2 K	305.3 K
6°	$u_{\mathrm{t,rce}} = u_{\mathrm{amc}}$, summer	13.0°	13.2°	14.1°	14.4°	13.0°	13.2°
	$u_{\mathrm{t,rce}} = u_{\mathrm{amc}}$, winter	-18.5°	-18.3°	-19.6°	-19.3°	-18.5°	-18.3°
	Equal area φ_{s}	24.1°	24.4°	25.6°	25.9°	24.0°	24.1°
	Equal area φ_{w}	-32.7°	-32.5°	-34.5°	-34.3°	-32.7°	-32.3°
	Equal area φ_{a}	18.1°	18.2°	18.8°	18.9°	18.1°	18.0°
	Equal area $\hat{\theta}_{\mathrm{a}}$ or $\theta_{\mathrm{eb,a}}$	303.4 K	303.3 K	303.0 K	303.0 K	303.4 K	303.4 K
23.5°	$u_{\mathrm{t,rce}} = u_{\mathrm{amc}}$, summer	23.5°	23.5°	23.5°	23.5°	23.5°	23.5°
	$u_{\mathrm{t,rce}} = u_{\mathrm{amc}}$, winter	-30.1°	-28.7°	-30.9°	-29.4°	-30.1°	-28.7°
	Equal area φ_{s}	35.9°	35.3°	38.1°	37.6°	36.1°	35.2°
	Equal area φ_{w}	-51.1°	-48.7°	-53.8°	-51.4°	-51.9°	-48.9°
	Equal area φ_{a}	34.5°	33.8°	36.4°	35.7°	34.7°	33.7°
	Equal area $\hat{\theta}_{\mathrm{a}}$ or $\theta_{\mathrm{eb,a}}$	304.7 K	304.8 K	304.2 K	304.3 K	304.6 K	304.8 K

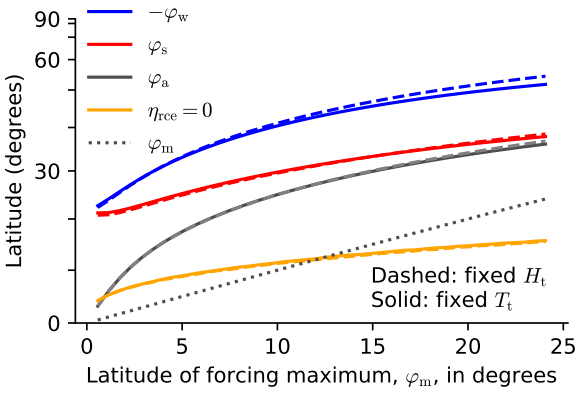

FIG. 4. Equal-area model solutions for the latitude of the poleward edges of the winter (φ_{w}; flipped in sign for easier visual comparison with the other metrics) and summer (φ_{s}) Hadley cells and their shared edge (φ_{a}), for φ_{m} ranging from 0.5 to 18°, with $\hat{\theta}_{\mathrm{amc}}$ derived with either the tropopause (dashed) height or (solid) temperature assumed constant. (Orange curves) latitude in the summer hemisphere where $\eta_{\mathrm{t,rce}} = 0$.

7. Numerically simulated and analytically approximated latitude-by-latitude RCE

The preceding sections indicate that nearly inviscid, axisymmetric Hadley cell theory is largely insensitive to how the tropopause height varies with latitude, at least under the given analytical profiles of the RCE thermal state. In principle, however, the tropopause treatment could be more influential when a more realistic latitude-by-latitude RCE state corresponding to Earth's actual insolation distribution is considered. And, as described in the Introduction, the accuracy of the fixed-T_{t} assumption as applied on a latitude-by-latitude basis requires additional consideration. This section addresses those concerns.

a. Model and simulations description

We use the single column model provided by the `climlab` package for the Python programming language (Rose 2018). Convection is represented by simple convective adjustment (Manabe and Wetherald 1967) to a specified lapse rate that we set to 0.65 times the dry adiabat as in the moist Boussinesq calculations above. Radiative transfer calculations use the RRTMG model (Mlawer et al. 1997). Relative humidity is prescribed, using the profile of Manabe and Wetherald (1967) (see their Eq. 2), which decreases in height from a surface value of 0.77 but is uniform horizontally and in time. The surface is a mixed layer ocean of 1 meter depth.[4] There are no surface turbulent fluxes; instead convective adjustment adjusts both atmospheric and surface temperatures, with the surface timescale dependent on the mixed-layer depth. Surface albedo is set to 0.3 in all columns.

Simulations are performed with time-invariant insolation representing present-day, annual-mean insolation sampled at latitude values separated by 1°, from 89.5°S to 89.5°N. Each is run for 3000 days, with averages taken over the last 2200 days, wherein a steady state has been reached (Cronin and Emanuel 2013). Each column has 100 evenly spaced pressure levels from the surface to 0 hPa. We emphasize that each latitude is its own single column simulation, with no communication across latitudes. The latitude value for each simulation is used to specify the insolation only; the single column model does

[4] A smaller mixed layer depth would lead to faster equilibration times, but at smaller depths instabilities can arise in highly insolated columns that cause the model to crash.

not account for rotational effects and is thus agnostic to the local Coriolis parameter.

From the equilibrated temperature profiles in each column, the tropopause is computed using several different metrics: the World Meteorological Organization definition of the lowest point at which the lapse rate reaches 2 K/km (WMO 1957); the "cold point tropopause", i.e. the coldest point in each column; and, c.f. Schneider and Walker (2006), the location where the vertical curvature in temperature, i.e. $\partial_{zz}T$, maximizes. A fixed-height tropopause definition is also computed using a value of 14 km, a value chosen by eye to be similar within the Tropics to the other tropopause definitions (results are insensitive to reasonable modifications of this value). On similarly ad-hoc grounds, we select the 214 K isotherm as the fixed-temperature tropopause; values closer to the 200 K used in the preceding analytical work yields too deep a tropopause in the Tropics (not shown) compared to the other definitions.

The gradient-balanced wind field is computed from the simulated temperature fields, using the expression for gradient balance in pressure coordinates. Assuming negligible surface wind, this is

$$u(p,\varphi) = \Omega a \cos\varphi \left(\sqrt{1 - \frac{1}{\cos\varphi \sin\varphi} \frac{R}{\Omega^2 a^2} \ln\left(\frac{p_0}{p}\right) \frac{\partial \hat{T}}{\partial \varphi}} - 1 \right)$$

where, in a slight deviation from the previous notation, $\hat{T}$ is the average temperature from the surface pressure (which is always set to $p_0 = 1000$ hPa), to the given pressure p (which above always corresponded to the tropopause pressure p_t, but here is more general, since p_t itself is dependent on which tropopause definition is being used).

To remove the distracting influence of gridpoint noise, we apply a 1-2-1 smoothing filter in latitude to the temperature field. Because the insolation and other boundary conditions are symmetric about the equator, we average the model output at each latitude across the northern and southern hemispheres after applying the smoothing but before computing the various tropopause definitions or the gradient wind.

b. Analytical approximation

To obtain an expression for the RCE fields that does not require any numerical model, we use the well-known planetary energy balance model with a one-layer greenhouse but applied at each latitude. Given the local top-of-atmosphere insolation S and albedo α, this yields a surface temperature of

$$T_s = 2^{1/4} \left[\frac{S(1-\alpha)}{\sigma} \right]^{1/4},$$

where σ is the Stefan-Boltzmann constant. The corresponding $u_{t,rce}$ field is then computed by first computing $\hat{\theta}_{rce}$ from (4) with $\gamma = 0.65$ and then using (3a) using $\theta_0 = 290$ K and assuming $H_{t,rce} = 12$ km, a lower value than that used for the fixed-H_t tropopause calculation chosen *ad hoc* to give the best agreement with the $u_{t,rce}$ fields inferred directly from the numerical simulation results.

c. Simulation and analytical results

Figure 5 shows the simulated equilibrium temperature distribution as a function of latitude and pressure, with the tropopause indicators overlaid. Unlike all the other tropopause definitions, the fixed-height tropopause is at the warmest temperatures and highest pressures in the tropics, as noted in the Introduction. All others generally become colder and at higher pressures moving toward the poles and are oriented with the curvature-based value below the WMO value, and both those somewhat below the cold point.

Qualitatively, the fixed-T_t assumption is largely borne out within the Tropics, in the sense that the given isotherm remains in the vicinity of the other, more conventional tropopause definitions from the equator to mid-latitudes. And the other tropopause definitions all occur at temperatures within 210-220 K within 30°S-30°N. At the same time, the fixed-T_t definition has the sharpest meridional drop of all, with near the highest values of all the definitions at the Equator, dropping to the lowest in the mid-latitudes, and then further dropping precipitously, nearly to the surface, at the poles.

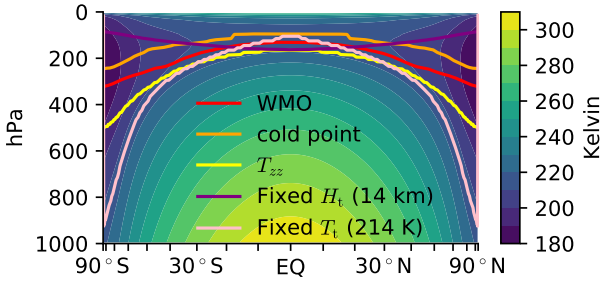

FIG. 5. (Filled contours) temperature in the single-column model simulations of latitude-by-latitude RCE with values as indicated in the colorbar. The overlaid thick contours are various definitions of the tropopause, with colors corresponding to the legend.

Figure 6 shows $u_{t,rce}$ as a function of latitude diagnosed at each of these tropopause definitions. All share a common overall structure, maximizing near the equator and decreasing mostly monotonically poleward Differences across the different definitions can exceed 30 m s^{-1} at some latitudes. However, in the subtropics where the $M_{t,rce} > \Omega a^2$ condition becomes no longer satisfied, the

$u_{t,rce}$ (and in turn $M_{t,rce}$) differences across definitions becomes more modest, and in fact the $M_{t,rce} = \Omega a^2$ point lies within 20.5-23.5° for all of them (not shown).

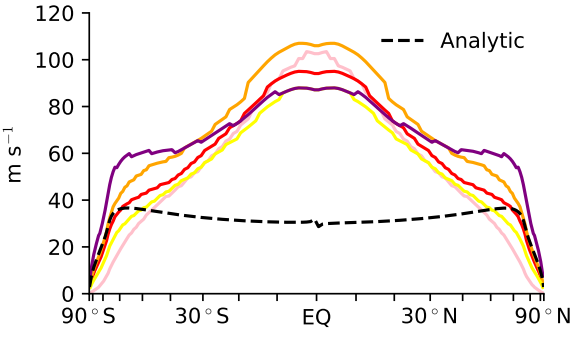

FIG. 6. $u_{t,rce}$ computed assuming negligible surface wind, using the temperature structure from the single-column model simulations of latitude-by-latitude RCE shown in Figure 5, and using various definitions of the tropopause as indicated by the legend in Figure 5, except for the dashed black curve, which corresponds to the simple analytical solution for surface temperature described in the main text, a tropopause height of 14 km, and a lapse rate of $\Gamma = \gamma\Gamma_d$, where $\gamma = 0.65$.

Overlaid on Figure 6 is the $u_{t,rce}$ value diagnosed from this simple analytical solution based on local top-of-atmosphere energy balance. Except at high latitudes, it is well removed from all of the different $u_{t,rce}$ computations using the simulation data, being far too weak. The analytical solution fails to capture the pronounced local maximum at the equator present in the simulations — biased low near the equator by ∼100 m s^{-1} (note that the small local maxima and minima straddling the equator are finite differencing artifacts). The insufficiently large values of the analytical $u_{t,rce}$ approximation in low- to mid-latitudes lead to its corresponding $M_{t,rce} = \Omega a^2$ criterion occurring well equatorward, at ∼14.5°, of any of the values taken from the simulations (not shown).

This failure of the analytical zonal wind can be better understood from Figure 7, which shows the troposphere-averaged temperature from the numerical solutions and potential temperature for the analytical solutions, the former assuming a uniform tropopause pressure of 200 hPa and the latter the same uniform tropopause height of 14 km used to compute $u_{t,rce}$; results are insensitive to reasonable variations in these parameters. Temperatures from the simple analytical model vary more smoothly with latitude than do the simulated temperatures everywhere apart from the high latitudes, and these smaller $\partial_\varphi \hat{T}$ values lead to weaker $u_{t,rce}$. Evidently, the interactions between convection and radiation lead to a greater increase in tropospheric temperature with surface warming than does simple top-of-atmosphere radiative balance. For the purpose of investigating Hadley cell dynamics, a more sophisticated analytical approach thus seems necessary.

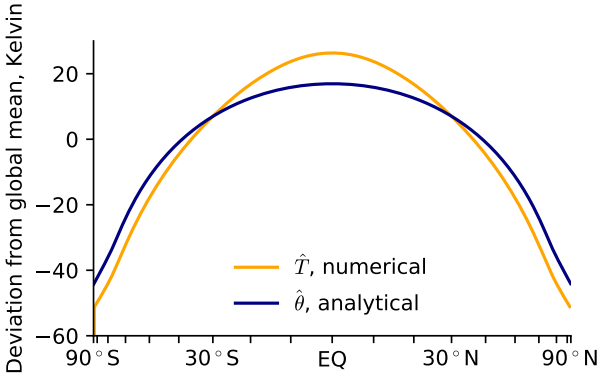

FIG. 7. Troposphere-averaged temperature from the single-column-model simulations and potential temperature from the simple analytical approximation (both in Kelvin). Both are presented as deviations from their respective global mean, since their meridional structure is of greater relevance than their absolute magnitude at any given latitude.

8. Summary

The classical axisymmetric theories of the Hadley cells — Hide's theorem, the angular momentum conserving (AMC) model, and the equal-area model — assume that the tropopause height (and with it the gradient-balanced zonal wind at the tropopause) are uniform in latitude in the absence of an overturning circulation, i.e. in latitude-by-latitude radiative-convective equilibrium (RCE), and unchanged by the emergence of the Hadley circulation. But recent work (Seeley et al. 2019b) suggests that the tropopause temperature is more nearly invariant than the tropopause height in RCE, at least on a domain-mean basis. Insofar as the tropopause temperature (and lapse rate) do not vary meridionally, the tropopause height must vary with surface temperature. We re-derive these axisymmetric theories assuming that the tropopause temperature is constant in latitude and across climate states. We then examine the tropopause temperature and Hadley cell metrics in numerical simulations of annual-mean, latitude-by-latitude RCE using a single column model.

If the tropopause temperature is uniform, under standard annual-mean and solsticial Newtonian cooling reference temperature profiles (Lindzen and Hou 1988) the RCE tropopause height can vary in latitude by ∼50% or more, being deepest where surface temperature is largest. Compared to if the tropopause height were uniform in latitude, the resulting gradient-balanced zonal wind at the tropopause can differ by up to tens of m s^{-1}, but over most of the domain the differences are modest, particularly in the subtropics. Differences between fixed-height and fixed-temperature calculations are largest in the winter hemisphere for solsticial forcing, and increase as the forcing maximum is moved toward the summer pole.

As such, the resulting influence on the absolute angular momentum and absolute vorticity fields, and with them

the range of supercritical forcing based on the conditions of Hide's theorem, are weakly modified, by $\lesssim 1^\circ$. This is both because of the modest magnitudes of the changes to $u_{\mathrm{t,rce}}$ and also to the fact that the Hide's theorem criteria typically stop being met in the subtropics, precisely where the fixed-temperature tropopause height approaches its tropical-mean value that seems the most appropriate value to use for fixed-height calculations: where the values of $u_{\mathrm{t,rce}}$ matter most for Hide's theorem, they are constrained to be least sensitive to the tropopause treatment.

The angular momentum conserving (AMC) zonal wind, u_{amc}, is determined by the ascent latitude φ_{a} and is a function of latitude but not height. It is thus unaltered by the tropopause treatment, but tropopause height variations consistent with a fixed T_{t} engender changes in the "critical" temperature field in gradient balance with that u_{amc} field. Specifically, a sharp subtropical shoulder in H_{t} causes $\hat{\theta}_{\mathrm{amc}}$ to also have a sharper shoulder than does the fixed-H_{t} calculation. When plugged into the equal-area model, this results in a trivial to modest equatorward contraction of the overall predicted Hadley circulation extent. Similar results for both the RCE and AMC quantities are found whether a dry or moist adiabat is assumed in the Boussinesq framework or if the CQE framework is used.

The tropopause temperature is reasonably uniform in latitude across the Tropics in single column model simulations sampling the full latitudinal range of Earth's annual mean insolation. As for the analytical results, $u_{\mathrm{t,rce}}$ and with it the Hide's theorem metrics are only modestly sensitive to the tropopause definition. The simulations generate temperature structures that are more sharply equatorially peaked than a simple analytical model based on local top-of-atmosphere energy balance, such that the $u_{\mathrm{t,rce}}$ field diagnosed from the analytical solution is separated from the simulated $u_{\mathrm{t,rce}}$ fields at most latitudes. Restricting to the simulated values, the minimal Hadley cell edge position from Hide's theorem varies across the tropopause definitions by only $\sim 2.5^\circ$.

9. Discussion

We have assumed identical lapse rates and tropopause temperatures in RCE and in the presence of a large-scale overturning circulation. However, the Hadley cells must generate some positive (moist) static stability that is not present in the RCE state in order to effect any net meridional energy transport and thus alter the depth-averaged temperature fields (Caballero et al. 2008). While this shallowing of the lapse rate going from RCE to the dynamically equilibrated state would not appear to alter the influence of the fixed-T_{t} assumption, it could in principle alter the equal-area solutions: at low latitudes, $\hat{\theta}$ will have increased overall, likely leading to a smaller meridional extent that conserves the $\hat{\theta}$ integral from the RCE state.

For moist atmospheres, even in the latitude-by-latitude RCE state some meridional variation in the lapse rate is likely, as can be seen from two largely independent lines of argument. First, c.f. Held (2000), convection will be deepest where insolation and surface temperatures are highest, which combined with the weak temperature gradient (WTG) constraint at low latitudes (e.g. Sobel et al. 2001) sets the lapse rate remotely also. The resulting static stability suppresses convection in columns with lower insolation and surface temperature, ultimately producing an inversion at the boundary layer top. Second, c.f. Emanuel (1995), if a significant fraction of a parcel's moisture is rained out in the ascending branch, then it will be forced to warm dry adiabatically over most of its return to the surface in the descending branch, setting up a different lapse rate between the two branches and leading to a decoupling between the boundary layer and the free troposphere in the descending branch.

Horizontal homogenization of temperature (or pressure) in low latitudes is the result of gravity waves and thus does not require any large-scale flow. In other words, latitude-by-latitude RCE should arguably reflect the influences of WTG, which we would expect to weaken $u_{\mathrm{t,rce}}$ and make it further insensitive to the tropopause treatment. Numerical simulations of latitude-by-latitude RCE such as ours in which each latitude is effectively its own single column simulation cannot account for this effect.

In light of the overall failure of the simplistic energy balance analytical solution to replicate the numerically simulated RCE results, it would be useful to consider other analytical solutions. We have in mind particularly that of Romps (2016), which also relies on an assumption of a fixed tropopause temperature of 200 K but accounts for far more processes than we do. Romps notes that the tropopause height rises more rapidly with surface temperature at higher surface temperatures. This would further increase the latitudinal variations in RCE tropopause height compared to our extremely simple assumption of a fixed lapse rate.

It is possible that sufficiently strong forcing or in planetary atmospheres sufficiently removed in parameter space from Earth's atmosphere, tropopause variations could make more of an impact that in the solutions we have presented for Earth under conventional forcings. But for Earth it seems clear that, regardless of the ongoing debate as to how relevant or not axisymmetric arguments even are in Earth's macroturbulent, strongly eddying atmosphere, the axisymmetric theory itself is quite insensitive to meridional tropopause variations. This should add (however modestly) to our confidence in classical, Boussinesq axisymmetric theory's utility: whatever its imperfections, classical axisymmetric theory's assumption of a fixed tropopause height is not an important one.

Acknowledgments. We thank Brian Rose for developing `climlab` and timely guidance in using it. S.A.H. was initially supported by NSF Atmospheric and Geospace Sciences Postdoctoral Research Fellowship (award #1624740) and subsequently by the Caltech Foster and Coco Stanback Postdoctoral Fellowship. S.B. was supported by NSF award AGS-1462544.

APPENDIX A

Physical relationship between Boussinesq and convective quasi-equilibrium atmospheres

The adaptation of axisymmetric Hadley cell theory from dry, Boussinesq atmospheres to moist, CQE atmospheres was first done by Emanuel (Emanuel et al. 1994; Emanuel 1995), but we expand the discussion here in order to clarify the connections between the two frameworks.

a. Gradient balance in CQE

The state of gradient balance in a CQE atmosphere may be expressed as

$$\left.\frac{\partial T}{\partial p}\right|_{s^*}\frac{\partial s_\mathrm{b}}{\partial \varphi}=\frac{1}{a^2}\frac{\sin\varphi}{\cos^2\varphi}\frac{\partial M^2}{\partial p}, \tag{A1}$$

where T is temperature, p is pressure, s^* is the saturation moist entropy, s_b is the subcloud moist entropy, and $M=a\cos\varphi(\Omega a\cos\varphi+u)$. The core assumption of CQE is that $s^*(p)\equiv s_\mathrm{b}$ at each latitude: convection is sufficiently frequent and vigorous as to make the time-mean stratification exactly moist adiabatic, with the saturation moist entropy at each height equal to the moist entropy of the subcloud air transported into the free troposphere by the convection. Integrating from the surface where $u\approx 0$ and thus $M\approx\Omega a^2\cos^2\varphi$ to the tropopause yields

$$(T_\mathrm{s}-T_\mathrm{t})\frac{\partial s_\mathrm{b}}{\partial\varphi}=\frac{1}{a^2}\frac{\sin\varphi}{\cos^2\varphi}(M^2-\Omega^2a^4\cos^4\varphi), \tag{A2}$$

where T_s is surface temperature and T_t is the tropopause temperature. Using the definitions of s_b and M, solving for u yields

$$u_\mathrm{t,rce}=\Omega a\cos\varphi\left[\sqrt{1-\frac{1}{\cos\varphi\sin\varphi}\frac{c_p(T_\mathrm{s}-T_\mathrm{t})}{\Omega^2a^2\theta_\mathrm{eb}}\frac{\partial\theta_\mathrm{eb}}{\partial\varphi}}-1\right]. \tag{A3}$$

This is nearly identical to (3a), but with gH/θ_0 replaced by $c_p(T_\mathrm{s}-T_\mathrm{t})/\theta_\mathrm{eb}$. As noted in Section 1, $T_\mathrm{s}-T_\mathrm{t}$ is effectively an expression of the tropopause height in temperature coordinates. This is most easily seen for a dry atmosphere in which $\Gamma=\Gamma_\mathrm{d}$; then $c_p(T_\mathrm{s}-T_\mathrm{t})=gH$. The $1/\theta_0$ term arises from the expression of hydrostatic balance in the Boussinesq model: $\partial_z\Phi=-(g/\theta_0)\theta$, where $\Phi=gz$ is geopotential, whereas the $1/\theta_\mathrm{eb}$ term in (A3) arises from the meridional derivative of moist entropy: $s\equiv c_p\ln\theta$, and thus $\partial_\varphi s=(1/\theta)\partial_\varphi\theta$.

b. AMC thermal fields in Boussinesq vs. CQE atmospheres

The CQE θ_eb distribution in gradient balance with u_amc is, c.f. Eq. 11 of Emanuel (1995),

$$\theta_\mathrm{eb}=\theta_\mathrm{eb,a}\exp\left[-\frac{\Omega^2a^2}{2c_p(T_\mathrm{s}-T_\mathrm{t})}\frac{(\cos^2\varphi_\mathrm{a}-\cos^2\varphi)^2}{\cos^2\varphi}\right], \tag{A4}$$

where θ_eb is the subcloud equivalent potential temperature, $\theta_\mathrm{eb,a}$ is the value of θ_eb at φ_a, and $T_\mathrm{s}-T_\mathrm{t}$ has been assumed constant. The exponential operator in (A4) arises from the use of entropy rather than potential temperature as the thermodynamic tracer (see e.g. Ch. 1 of Vallis (2017)). A first-order Taylor expansion of (A4) yields

$$\frac{\theta_\mathrm{eb}(\varphi)-\theta_\mathrm{ba}}{\theta_\mathrm{ba}}\approx-\frac{\Omega^2a^2}{2c_p(T_\mathrm{s}-T_\mathrm{t})}\frac{(\cos^2\varphi_\mathrm{a}-\cos^2\varphi)^2}{\cos^2\varphi}, \tag{A5}$$

Taking into consideration the Boussinesq-CQE mappings discussed in the previous subsection, we see that (A5) is essentially the same as (5a): the Boussinesq $\hat{\theta}_\mathrm{amc}$ amounts to a linearization about φ_a of its dry CQE counterpart.

The near-equivalence of (5a) and (A4) is demonstrated in Figure A8, which shows (5a) and (A4) over one hemisphere with forcing maxima of 0, 20, 40, 60, and 80°N, assuming $\theta_\mathrm{ba}=350$ K and $T_\mathrm{s}-T_\mathrm{t}=100$ K in the Emanuel (1995) solution, and with the Lindzen and Hou (1988) parameters $H=13$ km and $\theta_0=300$ K chosen subjectively and by eye to minimize the difference between the two models. Both versions are mirror-symmetric about the equator, with $\sim\cos^4\varphi$ dependence at the equator for $\varphi_\mathrm{a}=0^\circ$, thereby preventing equatorial westerlies. The Boussinesq solutions have the undesirable feature of passing through absolute zero, but the CQE cases likewise lose their physical meaningfulness as surface temperatures drop for a given T_t, certainly once $\theta_\mathrm{eb}\sim T_\mathrm{t}$.

We emphasize here that the CQE θ_eb quantity includes the effects of moisture, while the Boussinesq $\hat{\theta}$, even if the lapse rate is set to the "moist" value of $\gamma\Gamma_\mathrm{d}$ with $\gamma=0.65$, is troposphere-averaged dry potential temperature. In calculations of $u_\mathrm{t,rce}$ for the CQE framework, we take (2) to be an expression for the RCE θ_eb distribution, i.e. including the distribution of moisture. As such, the *dry* potential temperature fields differ between the Boussinesq and CQE frameworks, but to an extent that would require knowledge of the relative humidity and subcloud pressure level values, which we do not specify.

APPENDIX B

Derivation of angular momentum conserving T_s fields with fixed-T_t, Boussinesq

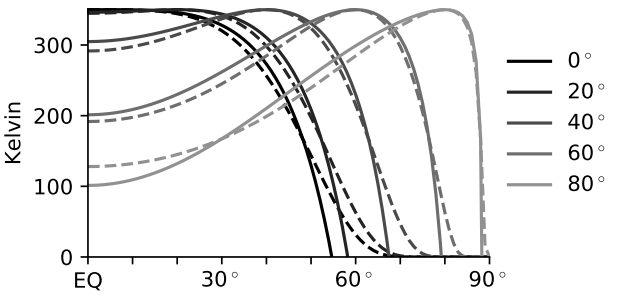

FIG. A8. (Solid curves) Boussinesq $\hat{\theta}_{\rm amc}$ fields given by (5a) and (dashed curves) CQE $\theta_{\rm eb,amc}$ fields given by (A4). Pairs of curves with the same gray shading are the solutions for a given $\varphi_{\rm a}$, ranging from 0° to 80° by 20° increments. In all cases the potential temperature value ($\hat{\theta}$ for Boussinesq, $\theta_{\rm eb,amc}$ for CQE) at the maximum is set to 350 K. For the CQE profiles, the difference between the surface and tropopause temperatures, $T_{\rm s}-T_{\rm t}$, is taken as a constant 100 K. The free parameters of the Lindzen and Hou (1988) profiles were then chosen subjectively to minimize the differences between the Lindzen and Hou (1988) and Emanuel (1995) solutions. In particular, the given tropospheric depth is 12 km, and the reference potential temperature is 290 K.

The starting point is Eq. 6 of Lindzen and Hou (1988), which expresses troposphere-averaged gradient balance. Using (1), this becomes:

$$\frac{\partial\hat{\theta}}{\partial\varphi}=\frac{\gamma\theta_0\Omega^2a^2}{c_p(T_{\rm s}-T_{\rm t})}\left(\frac{\sin\varphi}{\cos^3\varphi}\cos^4\varphi_{\rm a}-\cos\varphi\sin\varphi\right), \quad \text{(B1)}$$

where $\varphi_{\rm a}$ is the ascent latitude at which the temperature is maximal. Bringing the $T_{\rm s}-T_{\rm t}$ term to the opposite side and expanding yields

$$T_{\rm s}\frac{\partial\hat{\theta}}{\partial\varphi}-T_{\rm t}\frac{\partial\hat{\theta}}{\partial\varphi}=\frac{\gamma\theta_0\Omega^2a^2}{c_p}\left(\frac{\sin\varphi}{\cos^3\varphi}\cos^4\varphi_{\rm a}-\cos\varphi\sin\varphi\right). \quad \text{(B2)}$$

Using the chain rule, the left-hand-side can be expressed as

$$\frac{{\rm d}\hat{\theta}}{{\rm d}T_{\rm s}}\left(\frac{1}{2}\frac{\partial {T_{\rm s}}^2}{\partial\varphi}-T_{\rm t}\frac{\partial T_{\rm s}}{\partial\varphi}\right). \quad \text{(B3)}$$

For a constant lapse rate $\Gamma=\gamma\Gamma_{\rm d}$, it can be shown that

$$\frac{{\rm d}\hat{\theta}}{{\rm d}T_{\rm s}}=\frac{1}{2\gamma-1}\frac{{T_{\rm s}}^{1/\gamma-1}}{T_{\rm s}-T_{\rm t}}\left[(2\gamma-1){T_{\rm s}}^{2-1/\gamma}+\frac{(1-\gamma)T_{\rm s}-T_{\rm t}}{T_{\rm s}-T_{\rm t}}\left({T_{\rm s}}^{2-1/\gamma}-{T_{\rm t}}^{2-1/\gamma}\right)\right]. \quad \text{(B4)}$$

This is itself a function of $T_{\rm s}$ and γ. However, it varies almost linearly over the range $200<T_{\rm s}<350$ for $T_{\rm t}=200$ K and $\gamma=0.65$, from 1.27 to 1.43. So, for Earth-like settings, it can be treated as a constant to a good approximation. We use 1.4.

With this assumed constant factor, the above expression can be integrated directly in latitude, yielding

$$\frac{1}{2}{T_{\rm s}}^2-T_{\rm t}T_{\rm s}+T_{\rm t}T_{\rm sa}^2-\frac{1}{2}T_{\rm sa}-\frac{\gamma\theta_0\Omega^2a^2}{c_p{\rm d}\hat{\theta}/{\rm d}T_{\rm s}}\frac{(\cos^2\varphi_{\rm a}-\cos^2\varphi)^2}{\cos^2\varphi}=0, \quad \text{(B5)}$$

where $T_{\rm sa}$ is the value of $T_{\rm s}$ at $\varphi_{\rm a}$. Finally, this can be solved directly using the quadratic equation, yielding (5b).

APPENDIX C

Derivation and calculation of RCE and AMC fields with fixed-$T_{\rm t}$, CQE

Under the fixed-$T_{\rm t}$ assumption, a value for $T_{\rm s}$ is required both in (A3) above and in the derivation of $\theta_{\rm eb,amc}$ presented immediately below. As noted above, in the Boussinesq framework, unless the stratification is dry adiabatic, the troposphere-averaged potential temperature is larger than the surface temperature, and so an accurate diagnosis of $u_{\rm t,rce}$ and $\hat{\theta}_{\rm amc}$ requires inverting the expression for $\hat{\theta}$ numerically in order to solve for the true $T_{\rm s}$ value. Under CQE, a similar issue arises regarding how to infer $T_{\rm s}$ from $\theta_{\rm eb}$, but unlike the Boussinesq case there are two, canceling factors to consider.

On the one hand, the inclusion of moisture in the expression for $\theta_{\rm e}$ acts to make it larger than $T_{\rm s}$. On the other hand, we can expect a steeper-than-moist-adiabatic lapse rate below cloud base due to the relative dearth of condensation. This acts to make $T_{\rm s}$ warmer than it would be if the stratification was moist adiabatic all the way to the surface — the more so the steeper the lapse rate or the deeper the subcloud layer. Given the level of approximation we are working at, these (at least partially) canceling influences lead us to simply take $\theta_{\rm eb}\approx T_{\rm s}$. We have also performed the calculations by inverting $\theta_{\rm eb}$ for $T_{\rm s}$, for a range of plausible subcloud layer pressures and relative humidities and assuming $T_{\rm s}\approx T_{\rm b}$, and the results are not significantly altered (not shown).

Under this assumption, the $\theta_{\rm eb,amc}$ profile obeys

$$\theta_{\rm eb}-T_{\rm t}\ln\frac{\theta_{\rm eb}}{\theta_{\rm ba}}=\theta_{\rm ba}-\frac{\Omega^2a^2}{2c_p}\frac{(\cos^2\varphi_{\rm m}-\cos^2\varphi)^2}{\cos^2\varphi}. \quad \text{(C1)}$$

This is not readily solvable analytically but is so numerically via standard root-finding algorithms (in this case, Brent's method as implemented in the `scipy` package for the Python programming language, which is also used for all other numerical solutions elsewhere in this manuscript).

Figure C9 shows critical potential temperature profiles for three different fixed tropospheric depths and with varying depth for three different tropopause temperatures, in

all cases with $\varphi_a = 23.5°$ and $\theta_{ba} = 350$ K. The θ_{eb} distribution attained with varying tropopause temperature has less meridional curvature at the equator and a weaker equator-to-φ_m gradient than the original, fixed tropopause version. The default cases (orange solid and middle dashed curves) differ by roughly 3 K at the equator, with the fixed-T_t case warmer and thus with a smaller equator-to-maximum gradient. By construction, all curves are equal to θ_{bm} at φ_m.

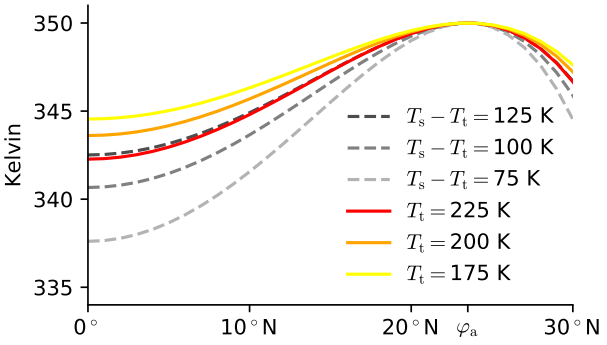

FIG. C9. Subcloud equivalent potential temperature profiles for which gradient wind balance yields AMC zonal wind at the tropopause in the convective quasi-equilibrium case, with an imposed maximum of $\theta_{ba} = 350$ K at $\varphi_m = 23.5°$. The dashed curves assume a fixed tropospheric depth; the solid curves assume fixed tropopause temperature and a surface temperature equal to the lowest level potential temperature. Within either category, different colors correspond to different assumed values of the free parameter, according to the legend.

References

Adam, O., and N. Paldor, 2010: Global Circulation in an Axially Symmetric Shallow-Water Model, Forced by Off-Equatorial Differential Heating. *J. Atmos. Sci.*, **67 (4)**, 1275–1286, doi:10.1175/2009JAS3324.1.

Caballero, R., R. T. Pierrehumbert, and J. L. Mitchell, 2008: Axisymmetric, nearly inviscid circulations in non-condensing radiative-convective atmospheres. *Q.J.R. Meteorol. Soc.*, **134 (634)**, 1269–1285, doi:10.1002/qj.271.

Cronin, T. W., and K. A. Emanuel, 2013: The climate time scale in the approach to radiative-convective equilibrium. *Journal of Advances in Modeling Earth Systems*, **5 (4)**, 843–849, doi:10.1002/jame.20049.

Emanuel, K. A., 1995: On Thermally Direct Circulations in Moist Atmospheres. *J. Atmos. Sci.*, **52 (9)**, 1529–1534, doi:10.1175/1520-0469(1995)052⟨1529:OTDCIM⟩2.0.CO;2.

Emanuel, K. A., J. David Neelin, and C. S. Bretherton, 1994: On large-scale circulations in convecting atmospheres. *Q.J.R. Meteorol. Soc.*, **120 (519)**, 1111–1143, doi:10.1002/qj.49712051902.

Fang, M., and K. K. Tung, 1994: Solution to the Charney Problem of Viscous Symmetric Circulation. *Journal of the Atmospheric Sciences*, **51 (10)**, 1261–1272, doi:10.1175/1520-0469(1994)051⟨1261:STTCPO⟩2.0.CO;2.

Hartmann, D. L., and K. Larson, 2002: An important constraint on tropical cloud - climate feedback. *Geophys. Res. Lett.*, **29 (20)**, 1951, doi:10.1029/2002GL015835.

Held, I. M., 1982: On the Height of the Tropopause and the Static Stability of the Troposphere. *J. Atmos. Sci.*, **39 (2)**, 412–417, doi:10.1175/1520-0469(1982)039⟨0412:OTHOTT⟩2.0.CO;2.

Held, I. M., 2000: The General Circulation of the Atmosphere. *The General Circulation of the Atmosphere: 2000 Program in Geophysical Fluid Dynamics*, No. WHOI-2001-03, Woods Hole Oceanog. Inst. Tech. Rept., Woods Hole Oceanographic Institution, 1–54.

Held, I. M., and A. Y. Hou, 1980: Nonlinear Axially Symmetric Circulations in a Nearly Inviscid Atmosphere. *J. Atmos. Sci.*, **37 (3)**, 515–533, doi:10.1175/1520-0469(1980)037⟨0515:NASCIA⟩2.0.CO;2.

Hide, R., 1969: Dynamics of the Atmospheres of the Major Planets with an Appendix on the Viscous Boundary Layer at the Rigid Bounding Surface of an Electrically-Conducting Rotating Fluid in the Presence of a Magnetic Field. *J. Atmos. Sci.*, **26 (5)**, 841–853, doi:10.1175/1520-0469(1969)026⟨0841:DOTAOT⟩2.0.CO;2.

Hill, S. A., S. Bordoni, and J. L. Mitchell, 2019: Axisymmetric Constraints on Cross-Equatorial Hadley Cell Extent. *J. Atmos. Sci.*, **76 (6)**, 1547–1564, doi:10.1175/JAS-D-18-0306.1.

Lindzen, R. S., and A. V. Hou, 1988: Hadley Circulations for Zonally Averaged Heating Centered off the Equator. *J. Atmos. Sci.*, **45 (17)**, 2416–2427, doi:10.1175/1520-0469(1988)045⟨2416:HCFZAH⟩2.0.CO;2.

Manabe, S., and R. T. Wetherald, 1967: Thermal Equilibrium of the Atmosphere with a Given Distribution of Relative Humidity. *J. Atmos. Sci.*, **24 (3)**, 241–259, doi:10.1175/1520-0469(1967)024⟨0241:TEOTAW⟩2.0.CO;2.

Mlawer, E. J., S. J. Taubman, P. D. Brown, M. J. Iacono, and S. A. Clough, 1997: Radiative transfer for inhomogeneous atmospheres: RRTM, a validated correlated-k model for the longwave. *Journal of Geophysical Research: Atmospheres*, **102 (D14)**, 16 663–16 682, doi:10.1029/97JD00237.

Plumb, R. A., and A. Y. Hou, 1992: The Response of a Zonally Symmetric Atmosphere to Subtropical Thermal Forcing: Threshold Behavior. *J. Atmos. Sci.*, **49 (19)**, 1790–1799, doi:10.1175/1520-0469(1992)049⟨1790:TROAZS⟩2.0.CO;2.

Romps, D. M., 2016: Clausius–Clapeyron Scaling of CAPE from Analytical Solutions to RCE. *J. Atmos. Sci.*, **73 (9)**, 3719–3737, doi:10.1175/JAS-D-15-0327.1.

Rose, B. E. J., 2018: CLIMLAB: A Python toolkit for interactive, process-oriented climate modeling. *The Journal of Open Source Software*, **3 (24)**, 659–660, doi:10.21105/joss.00659.

Schneider, E. K., 1977: Axially Symmetric Steady-State Models of the Basic State for Instability and Climate Studies. Part II. Nonlinear Calculations. *J. Atmos. Sci.*, **34 (2)**, 280–296, doi:10.1175/1520-0469(1977)034⟨0280:ASSSMO⟩2.0.CO;2.

Schneider, T., 2004: The Tropopause and the Thermal Stratification in the Extratropics of a Dry Atmosphere. *J. Atmos. Sci.*, **61 (12)**, 1317–1340, doi:10.1175/1520-0469(2004)061⟨1317:TTATTS⟩2.0.CO;2.

Schneider, T., 2006: The general circulation of the atmosphere. *Annu. Rev. Earth Planet. Sci.*, **34**, 655–688.

Schneider, T., and S. Bordoni, 2008: Eddy-Mediated Regime Transitions in the Seasonal Cycle of a Hadley Circulation and Implications for Monsoon Dynamics. *J. Atmos. Sci.*, **65 (3)**, 915–934, doi: 10.1175/2007JAS2415.1.

Schneider, T., and C. C. Walker, 2006: Self-Organization of Atmospheric Macroturbulence into Critical States of Weak Nonlinear Eddy–Eddy Interactions. *J. Atmos. Sci.*, **63 (6)**, 1569–1586, doi: 10.1175/JAS3699.1.

Seeley, J. T., N. Jeevanjee, W. Langhans, and D. M. Romps, 2019a: Formation of Tropical Anvil Clouds by Slow Evaporation. *Geophysical Research Letters*, **0 (0)**, doi:10.1029/2018GL080747.

Seeley, J. T., N. Jeevanjee, and D. M. Romps, 2019b: FAT or FiTT: Are Anvil Clouds or the Tropopause Temperature Invariant? *Geophysical Research Letters*, **0 (0)**, doi:10.1029/2018GL080096.

Singh, M. S., 2019: Limits on the extent of the solsticial Hadley cell: The role of planetary rotation. *J. Atmos. Sci.*, doi:10.1175/JAS-D-18-0341.1.

Sobel, A. H., J. Nilsson, and L. M. Polvani, 2001: The Weak Temperature Gradient Approximation and Balanced Tropical Moisture Waves. *Journal of the atmospheric sciences*, **58 (23)**, 3650–3665.

Thompson, D. W. J., S. Bony, and Y. Li, 2017: Thermodynamic constraint on the depth of the global tropospheric circulation. *PNAS*, **114 (31)**, 8181–8186, doi:10.1073/pnas.1620493114.

Thompson, D. W. J., P. Ceppi, and Y. Li, 2018: A Robust Constraint on the Temperature and Height of the Extratropical Tropopause. *J. Climate*, **32 (2)**, 273–287, doi:10.1175/JCLI-D-18-0339.1.

Vallis, G. K., 2017: *Atmospheric and Oceanic Fluid Dynamics: Fundamentals and Large-Scale Circulation*. 2nd ed., Cambridge University Press.

Walker, C. C., and T. Schneider, 2005: Response of idealized Hadley circulations to seasonally varying heating. *Geophys. Res. Lett.*, **32 (6)**, L06 813, doi:10.1029/2004GL022304.

Walker, C. C., and T. Schneider, 2006: Eddy Influences on Hadley Circulations: Simulations with an Idealized GCM. *J. Atmos. Sci.*, **63 (12)**, 3333–3350, doi:10.1175/JAS3821.1.

WMO, 1957: Meteorology — a three-dimensional science. *WMO Bulletin*, **6 (4)**, 134–138.